The Astrophysical Journal, 622:106–115, 2005 March 20

DISCOVERY OF TWO GRAVITATIONALLY LENSED QUASARS WITH IMAGE SEPARATIONS OF 3″ FROM THE SLOAN DIGITAL SKY SURVEY

Masamune Oguri,[1,2] Naohisa Inada,[3] Joseph F. Hennawi,[1,4,5] Gordon T. Richards,[1] David E. Johnston,[1] Joshua A. Frieman,[6,7] Bartosz Pindor,[8] Michael A. Strauss,[1] Robert J. Brunner,[9] Robert H. Becker,[10,11] Francisco J. Castander,[12] Michael D. Gregg,[10,11] Patrick B. Hall,[13] Hans-Walter Rix,[14] Donald P. Schneider,[15] Neta A. Bahcall,[1] Jonathan Brinkmann,[16] and Donald G. York[6,17]

Received 2004 November 9; accepted 2004 December 7

ABSTRACT

We report the discovery of two doubly imaged quasars, SDSS J100128.61+502756.9 and SDSS J120629.65+433217.6, at redshifts of 1.838 and 1.789, and with image separations of 2.″86 and 2.″90, respectively. The objects were selected as lens candidates from the Sloan Digital Sky Survey (SDSS). Based on the identical nature of the spectra of the two quasars in each pair and the identification of the lens galaxies, we conclude that the objects are gravitational lenses. The lenses are complicated; in both systems there are several galaxies in the fields very close to the quasars, in addition to the lens galaxies themselves. The lens modeling implies that these nearby galaxies contribute significantly to the lens potentials. On larger scales, we have detected an enhancement in the galaxy density near SDSS J100128.61+502756.9. The number of lenses with image separation of $\sim 3''$ in the SDSS already exceeds the prediction of simple theoretical models based on the standard Λ-dominated cosmology and observed velocity function of galaxies.

Subject headings: cosmology: observations — cosmology: theory — gravitational lensing — quasars: individual (SDSS J100128.61+502756.9, SDSS J120629.65+433217.6)

1. INTRODUCTION

In strong gravitational lensing of quasars, the separation between multiple images, θ, is the most important observable linking observations to theory. Since the image separation is determined by the potential depth of the lens, the image separation distribution of lensed quasars offers a direct probe of the hierarchical structure of the universe. For instance, normal galaxies can produce strongly lensed quasars with image separations of $\sim 1''$, while lenses with image separation $>10''$ can only be caused by clusters of galaxies. About 70 examples of $\sim 1''$ lenses are known to date,[18] and there is one example of a lensed quasar system in which the lens potential is dominated by that of dark matter (Inada et al. 2003b; Oguri et al. 2004a).

Among gravitationally lensed quasars, those with intermediate image separations ($3'' \lesssim \theta \lesssim 7''$) are of great interest because they represent a link between small and large separation lenses. In the standard modeling procedure used to predict the distribution of image separations, assuming isothermal profiles and an a priori velocity function of galaxies, lenses with image separations $\gtrsim 3''$ are very rare, because even the largest early-type galaxies do not have Einstein radii this large. Thus, the probability for $\sim 7''$ lensing is almost negligible. However, while Q0957+561 ($\theta = 626$; Walsh et al. 1979) is primarily lensed by a galaxy, the image separation is boosted by the cluster in which the lensing galaxy resides. This example implies that the environment of the lens galaxy may significantly affect the distribution of image separations in the $3''$–$7''$ range (Keeton et al. 2000; Martel et al. 2002). In addition, a secondary mass along the line of sight could affect strong lensing (Wambsganss et al. 2005), and this also may enhance the lensing probabilities in this image separation range. Finally, there is a predicted contribution in this range from clusters; simple theoretical models that include transition of the property of lenses at $\sim 10^{13}\ M_\odot$ (e.g., Oguri 2002) predict that large separation lenses due to clusters begin to dominate the total lensing probability. Therefore, the overall lensing probability distribution for $\theta \gtrsim 3''$ is predicted to depend on the interplay of these two effects: the environmental effects and the emergence of cluster lenses. However, the overall lensing probability at $\theta \gtrsim 3''$ is quite small; thus a large number of quasars are needed to investigate the lensing probability distribution. Indeed, even the current largest homogeneous sample of lensed

[1] Princeton University Observatory, Peyton Hall, Princeton, NJ 08544.
[2] Department of Physics, University of Tokyo, Hongo 7-3-1, Bunkyo-ku, Tokyo 113-0033, Japan.
[3] Institute of Astronomy, University of Tokyo, 2-21-1 Osawa, Mitaka, Tokyo 181-8588, Japan.
[4] Department of Astronomy, University of California at Berkeley, 601 Campbell Hall, Berkeley, CA 94720-3411.
[5] Hubble Fellow.
[6] Astronomy and Astrophysics Department, University of Chicago, 5640 South Ellis Avenue, Chicago, IL 60637.
[7] Fermi National Accelerator Laboratory, P.O. Box 500, Batavia, IL 60510.
[8] Canadian Institute for Theoretical Astrophysics, University of Toronto, 60 St. George Street, Toronto, ON M5S 3H8, Canada.
[9] Department of Astronomy, University of Illinois, 1002 West Green Street, Urbana, IL 61801.
[10] Department of Physics, University of California at Davis, 1 Shields Avenue, Davis, CA 95616.
[11] Institute of Geophysics and Planetary Physics, Lawrence Livermore National Laboratory, L-413, 7000 East Avenue, Livermore, CA 94550.
[12] Institut d'Estudis Espacials de Catalunya/CSIC, Gran Capita 2-4, 08034 Barcelona, Spain.
[13] Department of Physics and Astronomy, York University, 4700 Keele Street, Toronto, ON M3J 1P3, Canada.
[14] Max-Planck Institute for Astronomy, Königstuhl 17, D-69117 Heidelberg, Germany.
[15] Department of Astronomy and Astrophysics, Pennsylvania State University, 525 Davey Laboratory, University Park, PA 16802.
[16] Apache Point Observatory, P.O. Box 59, Sunspot, NM 88349.
[17] Enrico Fermi Institute, University of Chicago, 5640 South Ellis Avenue, Chicago, IL 60637.

[18] A summary of known lensed quasar systems is available on the CASTLES home page (C. S. Kochanek, E. E. Falco, C. Impey, J. Lehar, B. McLeod, & H.-W. Rix) at http://cfa-www.harvard.edu/castles.

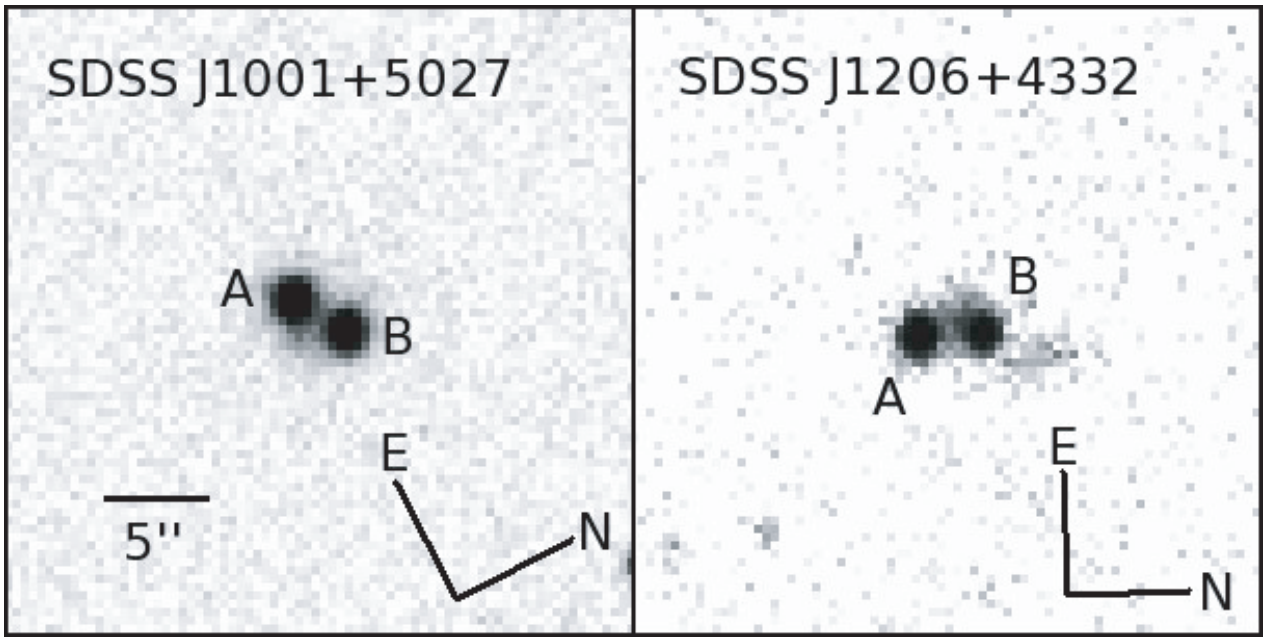

FIG. 1.—SDSS *i*-band images of SDSS J1001+5027 (*left*) and SDSS J1206+4332 (*right*). The image scale is 0.″396 pixel^{-1}.

quasars (Myers et al. 2003; Browne et al. 2003) contains only one lens in this image separation range.

In this paper, we present the discovery of two $\sim 3''$ gravitationally lensed quasars, SDSS J100128.61+502756.9 (hereafter SDSS J1001+5027) and SDSS SDSS J120629.65+433217.6 (hereafter SDSS J1206+4332). These gravitational lenses were identified from an ongoing lens search using the data of the Sloan Digital Sky Survey (SDSS; York et al. 2000; Stoughton et al. 2002; Abazajian et al. 2003, 2004, 2005). Currently the SDSS contains more than 50,000 spectroscopically classified quasars; thus the SDSS provides the opportunity to construct the largest homogeneous lens catalog in existence. Indeed, 13 new gravitationally lensed quasars have been found by using the SDSS (e.g., Inada et al. 2003a). In this paper, we describe photometric and spectroscopic observations of two new lens candidates and show that they are gravitational lenses. We model the lens systems and discuss the environments of the lens galaxies. We also compare the image separation distributions of lensed quasars in the SDSS (although still very preliminary because of the limited statistics) with a simple theoretical model.

This paper is organized as follows. In § 2 we briefly describe our method of searching for lens candidates from the SDSS data. Section 3 presents the results of both photometric and spectroscopic follow-up observations, and § 4 shows the result of lens modeling. Section 5 is devoted to a discussion of the environments of the lens galaxies. We also discuss the lensing probability distribution, which is shown in § 6. We summarize our results in § 7.

2. SELECTING CANDIDATES FROM THE SDSS DATA

All of the gravitational lenses presented in this paper were selected as lens candidates from the SDSS, which is a survey to image 10^4 deg^2 of the sky. The SDSS also conducts spectroscopy of galaxies and quasars that are selected from the imaging data (Eisenstein et al. 2001; Strauss et al. 2002; Richards et al. 2002; Blanton et al. 2003). A dedicated 2.5 m telescope at Apache Point Observatory (APO) is equipped with a multi-CCD camera (Gunn et al. 1998) with five optical broad bands centered at 3551, 4686, 6166, 7480, and 8932 Å (Fukugita et al. 1996; Stoughton et al. 2002). The imaging data are automatically reduced by the photometric pipeline (Lupton et al. 2001). The astrometric positions are accurate to about 0.″1 for sources brighter than $r = 20.5$ (Pier et al. 2003), and the photometric errors are typically less than 0.03 mag (Hogg et al. 2001; Smith et al. 2002; Ivezić et al. 2004). The spectra cover 3800–9200 Å at a resolution of 1800–2100.

We use spectroscopically classified quasars with $z > 0.6$ to search for gravitational lens candidates. SDSS J1001+5027 and SDSS J1206+4332 are identified as lens candidates by our standard candidate selection algorithm (N. Inada et al. 2005, in preparation). This algorithm is based on the idea that the image of a quasar pair with a small separation appears to be more extended than that of a single quasar and characterizes the extent by the following SDSS image parameters: dev_L (the likelihood that the image of the object is fitted by a de Vaucouleurs profile), exp_L (the likelihood that the image is fitted by an exponential disk), and star_L (the likelihood that the image is fitted by the point-spread function [PSF]). This algorithm has already found six new SDSS lenses (Inada et al. 2003a, 2005a, 2005b; Pindor et al. 2004, B. Pindor et al. 2005, in preparation; Oguri et al. 2004b) as well as all previously known gravitational lenses in the SDSS footprint. However, the possible second lensed components of the candidates we study in this paper were also recognized as separate astronomical objects in the SDSS imaging data because of the relatively large image separations (Pindor et al. 2003).

Figure 1 shows the SDSS *i*-band images of the candidates. In both images, the seeing was $\sim 1.''2$, better than the typical seeing of SDSS images, 1.″35 (Abazajian et al. 2003). The figure clearly shows two stellar components in each case; we designate the brighter ones as component A and the fainter ones as component B. Table 1 summarizes the result of the SDSS photometry of the components. In each system, the components have colors similar to each other and the colors are consistent with that expected from quasars; this makes them excellent lens candidates.

3. FOLLOW-UP OBSERVATIONS

Follow-up spectroscopic observations were conducted on 2003 November 20 and 2004 June 21 with the Double Imaging

TABLE 1
SDSS Astrometry and Photometry

Object	R.A. (J2000.0)	Decl. (J2000.0)	u	g	r	i	z
SDSS J1001+5027							
A	10 01 28.61	+50 27 56.9	17.71 ± 0.02	17.60 ± 0.02	17.55 ± 0.03	17.36 ± 0.03	17.33 ± 0.04
B	10 01 28.35	+50 27 58.5	18.60 ± 0.08	18.35 ± 0.08	18.11 ± 0.06	17.71 ± 0.06	17.62 ± 0.05
SDSS J1206+4332							
A	12 06 29.65	43 32 17.6	18.66 ± 0.03	18.80 ± 0.05	18.75 ± 0.05	18.53 ± 0.04	18.48 ± 0.04
B	12 06 29.65	43 32 20.6	19.69 ± 0.08	19.43 ± 0.12	19.33 ± 0.08	19.22 ± 0.08	18.83 ± 0.04

Notes.—Units of right ascension are hours, minutes, and seconds, and units of declination are degrees, arcminutes, and arcseconds. PSF magnitudes returned by the SDSS photometric pipeline are shown. Reddening corrections are not applied.

Spectrograph (DIS) on the Astrophysical Research Consortium (ARC) 3.5 m telescope at APO. We used a 1.″5 slit in low- (blue) or medium- (red) resolution mode. The resolution is about 2000. The final spectra cover the wavelength range of 3900–9400 Å. We aligned the slit along the direction joining the two images; since the separations between the images are large compared with the seeing size, extraction of the spectrum of each component was straightforward. The data were reduced using standard IRAF[19] reduction procedures.

We also obtained deep images of the systems with the 8k Mosaic CCD camera of the University of Hawaii 2.2 m telescope (UH88) at Mauna Kea and with the Seaver Prototype Imaging Camera (SPIcam) of the ARC 3.5 m telescope. The UH88 imaging was conducted on 2004 May 23 and 25. We obtained *VRI*-band images in the photometric nights; the exposure times were 360 s for each candidate and each band. The image scale was 0.″232 pixel^{-1}. We estimated the seeing as ∼0.″8, better than the SDSS seeing size of ∼1.″2. The ARC z-band imaging was conducted on 2004 January 13. The exposure was 300 s, the seeing was ∼1.″0, and the image scale was 0.″282 pixel^{-1}. Each frame was bias-subtracted and flat-field–corrected. The magnitudes in the UH88 images were calibrated by the standard star PG 1528+ 062 (Landolt 1992). Astrometry and photometry of the UH88 images are summarized in Table 2.

[19] IRAF is distributed by the National Optical Astronomy Observatory, which is operated by the Association of Universities for Research in Astronomy, Inc., under cooperative agreement with the National Science Foundation.

3.1. *SDSS J1001+5027*

Spectra and images of this object are shown in Figures 2 and 3, respectively. In Figure 2, both components show C IV, C III, and Mg II emission lines redshifted by $z = 1.838$. It is worth noting that the flux ratios (B/A) of the emission lines, particularly the C IV emission lines, are larger than that of the continuum; the equivalent widths of C IV emission lines are 56 and 76 Å for A and B, respectively. Such differences can be caused by the difference of the emission regions of continuum and broad emission lines combined with microlensing by stars. We find two extended objects near the quasar images (see Fig. 3; the image separation is 2.″86). When subtracting a quasar component, we used a nearby star as a PSF template. The objects, denoted by G1 and G2, have colors consistent with those of early-type galaxies at $0.2 \lesssim z \lesssim 0.5$ (Fukugita et al. 1995). Since galaxy G1 is nearly colinear with the two quasar components, it is likely that G1 is the main contributor to the lens potential. However, galaxy

TABLE 2
UH88 Astrometry and Photometry

Object	x (arcsec)[a]	y (arcsec)[a]	V[b]	R[b]	I[b]
SDSS J1001+5027					
A	0.000 ± 0.005	0.000 ± 0.005	18.12 ± 0.01	17.69 ± 0.01	17.32 ± 0.01
B	2.418 ± 0.009	1.526 ± 0.005	18.53 ± 0.01	17.98 ± 0.01	17.48 ± 0.01
G1	1.779 ± 0.049	0.857 ± 0.123	...	20.51 ± 0.03	19.63 ± 0.03
G2	1.795 ± 0.088	−0.700 ± 0.053	...	20.91 ± 0.04	20.15 ± 0.03
G1+G2[c]	...	...	22.09 ± 0.08	...	...
SDSS J1206+4332					
A	0.000 ± 0.011	0.000 ± 0.010	18.63 ± 0.02	18.54 ± 0.01	18.05 ± 0.02
B	−0.098 ± 0.006	2.894 ± 0.009	19.12 ± 0.02	18.95 ± 0.02	18.38 ± 0.02
G1	−0.664 ± 0.137	1.748 ± 0.028	...	21.34 ± 0.07	19.51 ± 0.03
G2	1.320 ± 0.147	5.999 ± 0.148	22.43 ± 0.13	21.16 ± 0.08	19.63 ± 0.04
G3	−2.052 ± 0.200	2.397 ± 0.152	21.78 ± 0.09	22.05 ± 0.10	22.57 ± 0.11

[a] Positions relative to the brighter quasar components are presented. The positive directions of x and y are defined by west and north, respectively. Error bars do not include the error of the image scale.
[b] Error bars do not include the zero-point error of ∼0.1 mag.
[c] In the V-band image it was difficult to decompose G1 and G2 because of the faintness of the image; thus, we show the total magnitude of these two galaxies.

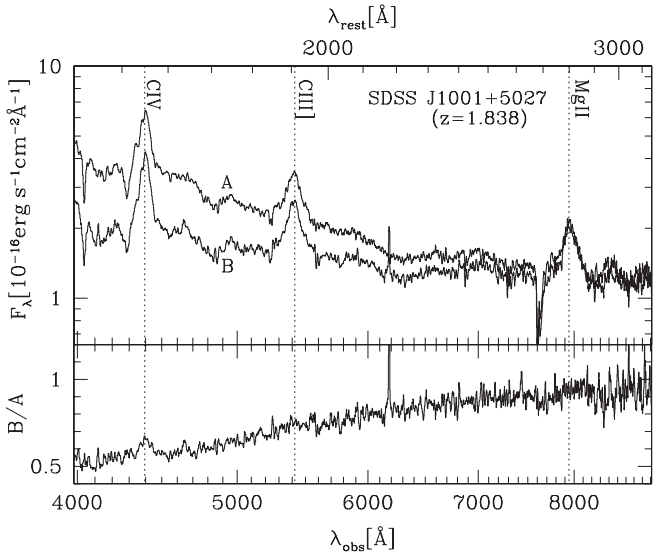

FIG. 2.—ARC 3.5 m spectra of SDSS J1001+5027 components A and B. The exposure time was 900 s. Both components have the same redshift, $z = 1.838$. The strong absorption at ~7600 Å is atmospheric. The feature at ~6200 Å is a bad column. The spectrum is smoothed by a 3 pixel boxcar. The ratio of the spectra as a function of wavelength is shown in the bottom panel. B is evidently reddened.

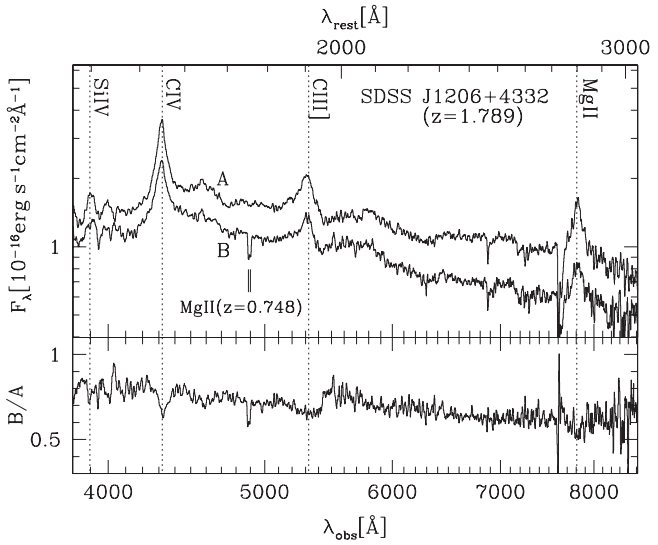

FIG. 4.—ARC 3.5 m spectra of components A and B of SDSS J1206+4332. The exposure time was 1800 s. The redshifts of both components are the same, $z = 1.789$. The strong absorption at ~7600 Å is atmospheric. The spectrum is smoothed by a 3 pixel boxcar. There is strong Mg II absorption at ~4900 Å (which corresponds to an absorber at $z = 0.748$) in the spectrum of component B. The ratio of the spectra as a function of wavelength is shown in the bottom panel.

G2 is also quite close to the lens system and could affect the lens potential significantly. We note that component B could be reddened by the lens galaxy G1.

3.2. *SDSS J1206+4332*

The spectra of the two components shown in Figure 4 show Si IV, C IV, C III, and Mg II emission lines at the same wavelengths, which supports the idea that this is a gravitationally lensed quasar at $z = 1.789$. However, the flux ratios (B/A) of the emission lines are slightly smaller than that of the continuum; the equivalent widths of C IV emission lines are 69 and 53 Å for A and B, respectively. The images in Figure 5 clearly reveal the lensing galaxy G1 as well as two quasar components separated by 2.″90, further supporting the lensing hypothesis. We also found other galaxies G2 and G3 near component B. These galaxies, particularly G2, may contribute to the lens potential to some extent. Indeed, both G1 and G2 are quite red (see Table 2) and are consistent with being high-redshift ($z \gtrsim 0.7$) early-type galaxies (Fukugita et al. 1995), while G3 is blue and thus may be a chance superposition of a local galaxy. There is strong Mg II absorption (equivalent width >2 Å) at ~4900 Å in the spectrum of component B. The redshift of the absorber is

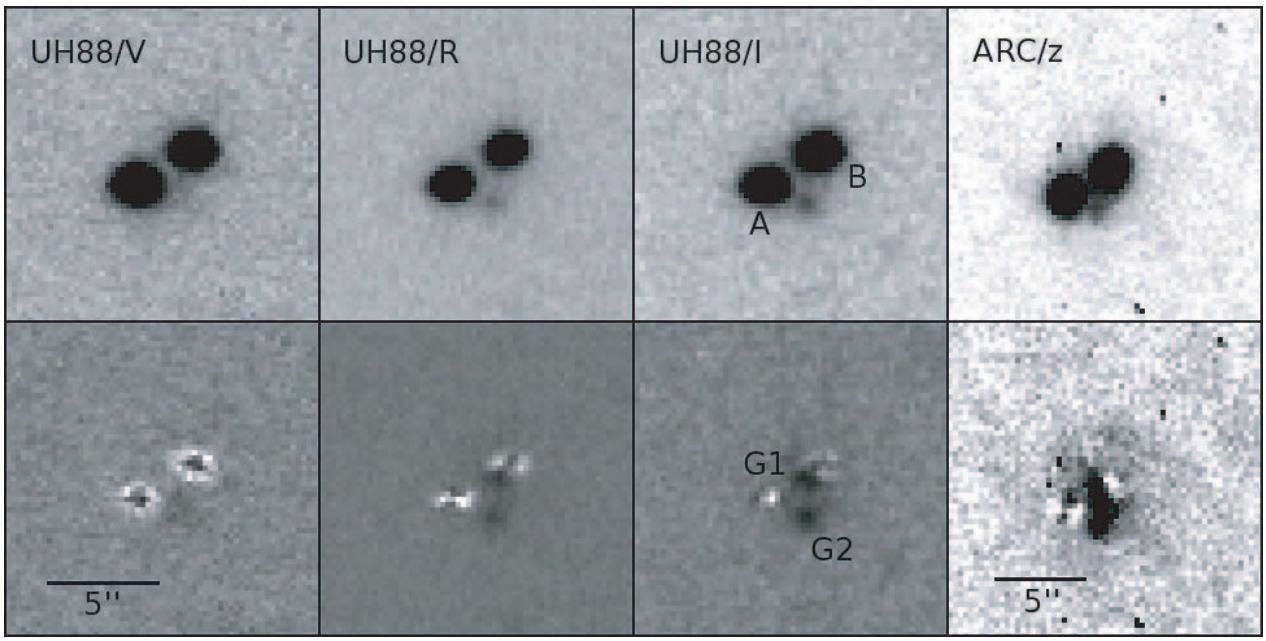

FIG. 3.—UH88 and ARC 3.5 m images of SDSS J1001+5027. Bottom panels are same as top panels, but after subtracting two point source quasar components. The image scales are 0.″232 pixel^{-1} (UH88) and 0.″282 pixel^{-1} (ARC), and the seeings were ~0.″8 (UH88) and ~1.″0 (ARC). North is up, and east is to the left in all panels. We find two galaxies in the residual images shown in the bottom panels, which are labeled G1 and G2.

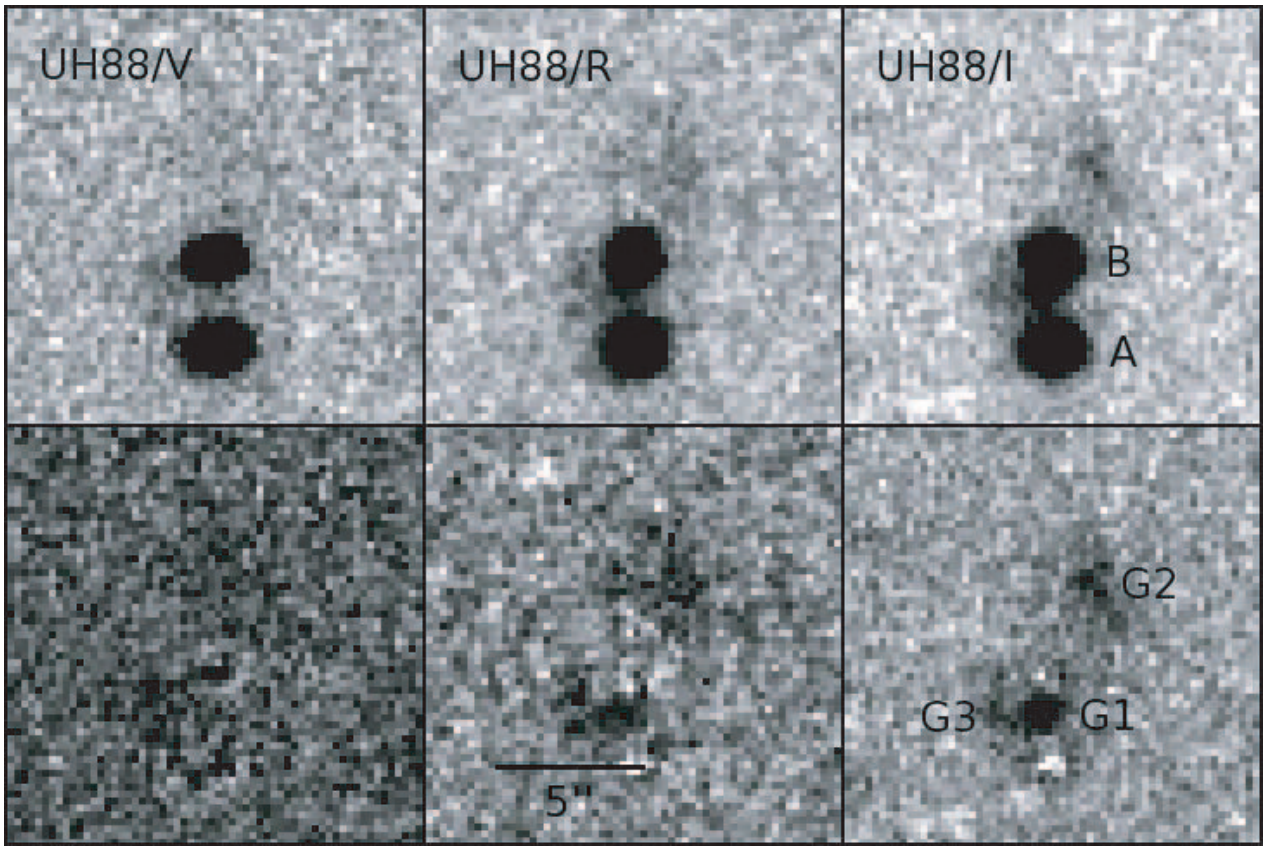

FIG. 5.—UH88 images of SDSS J1206+4332. Bottom panels show images after subtracting the two quasar components. North is up, and east is to the left in all panels. We find three galaxies in the residual images shown in the bottom panels, which are labeled G1, G2, and G3.

$z = 0.748$, consistent with the color of G1. Therefore the absorber may be associated with the lensing galaxy G1.

4. LENS MODELING

Although the lens systems appear quite complex, we first attempt to model the lens systems with simple models. Specifically, we try models that describe G1 by a Singular Isothermal Ellipsoid (SIE), or Singular Isothermal Sphere (SIS) plus external shear. Even these simple models, however, have eight parameters (the galaxy position x_g and y_g, the Einstein ring radius $R_{\rm E}$, the ellipticity e or shear γ, the position angle θ_e or θ_γ, the source position x_s and y_s, and the flux of the quasar f), which is equal to the number of observational constraints from the UH88 imaging data (the image positions, the galaxy position, and fluxes of the images; see Table 2). Thus, there are no degrees of freedom, and in usual cases we will be able to find models that perfectly reproduce the observables. To fit the models, we use standard lens modeling techniques as implemented in the *lensmodel* software (Keeton 2001).

SDSS J1001+5027 is well fitted by both the SIS plus shear and SIE models. The resulting fitting parameters are shown in Table 3. The ellipticity $e = 0.25$ in the SIE model is similar to that of the light, although the position angle $\theta_e = 10.9$ (measured east of north) is quite different from that of the light ($\sim -60^\circ$) measured from the UH88 image. In general the position angles of the light and lens models are aligned (Keeton et al. 1998); therefore this result suggests that the external field, rather than the galaxy G1, is responsible for the quadrupole moment of the lens potential. The position angles in the models are rather close to the direction to G2. Since in general the position angle of external shear gives an idea of the direction to a main perturber, it seems that G2 significantly affects the lens models. We also predict the time delay as $\Delta t \sim 45\ h^{-1}$ day (A leads B), assuming a lens redshift of $z = 0.3$.

Fitting SDSS J1206+4332 by either SIS plus shear or SIE failed; the models yielded large χ^2 values, $\chi^2 > 2$ with no degrees of freedom, and the models required unnaturally large e or γ. We also tried an SIE plus shear model, but the resulting fit was similarly poor. This implies that the lens system is too complicated to be described by such simple models. Thus, we add G2, which is modeled by an SIS, as well as galaxy G1 modeled by SIE, in order to make the model more realistic. We

TABLE 3
LENS MODELING

Model	$R_{\rm E}$ (arcsec)	e or γ	θ_e or θ_γ (deg)[a]	Δt (h^{-1} day)[b]
SDSS J1001+5027				
SIS+shear	1.35	0.09	11.9	42.4
SIE	1.38	0.25	10.9	47.0
SDSS J1206+4332				
SIE+G2[c]	1.39	0.31	−89.3	92.6

NOTE.—See § 4 for details of the lens models adopted here.
[a] Each position angle is measured east of north.
[b] For the redshifts of lens galaxies, we assumed a lens redshift of $z = 0.3$ for SDSS J1001+5027, and the redshift of strong Mg II absorption, $z = 0.748$, for SDSS J1206+4332. We also assumed $\Omega_M = 0.3$ and $\Omega_\Lambda = 0.7$, but the values are quite insensitive to these cosmological parameters.
[c] The Einstein radius of G2, $R_{\rm E}$(G2), is fixed to $1''$.

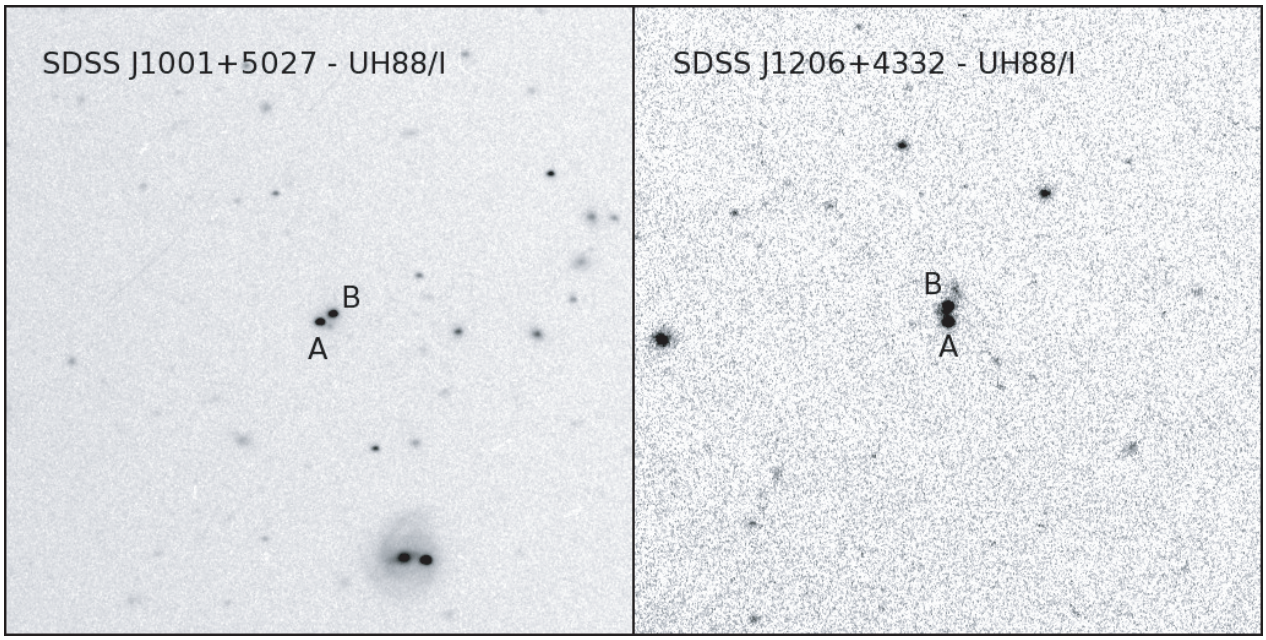

FIG. 6.—The $2' \times 2'$ *I*-band fields around the lens system SDSS J1001+5027 (*left*) and SDSS J1206+4332 (*right*) taken at UH88. The exposure times were both 360 s. North is up, and east is to the left in both panels.

derive best-fit models by changing the value of the Einstein radius of G2, $R_{\rm E}$(G2). We find that this "SIE+G2" model fits the data well when $R_{\rm E}({\rm G2}) \lesssim 1''$, although the maximum value is slightly smaller than that inferred from the Faber-Jackson relation [$R_{\rm E}({\rm G2})/R_{\rm E}({\rm G1}) = 0.92$ from the *R*-band flux ratio, assuming G1 and G2 are at the same redshift]. As a specific example, we show the best-fit parameters for $R_{\rm E}({\rm G2}) = 1''$ in Table 3. The position angle of galaxy G1 in the model ($\theta_e = -89.3$) is in good agreement with that observed. The time delay is derived to be $\Delta t = 92.6\ h^{-1}$ day (A leads B), assuming that the strong Mg II absorption system at $z = 0.748$ is associated with the lens galaxy. Even if we decrease the value of $R_{\rm E}$(G2) up to 0.″1, the time delay is affected only moderately; the time delay is predicted to be 104.4 h^{-1} day when $R_{\rm E}({\rm G2}) = 01$.

In summary, lens modeling has revealed that neither system is simple. In particular, the secondary galaxies may play an important role in both lenses.

5. LENS GALAXY ENVIRONMENTS

Lens galaxies of lensed quasars, particularly in systems with relatively large image separations ($\gtrsim 3''$), commonly lie in groups or clusters (Keeton et al. 2000; Faure et al. 2004). Such "compound" lens systems include Q0957+561 (Walsh et al. 1979), PG 1115+080 (Weymann et al. 1980), MG 2016+112 (Lawrence et al. 1984), RX J0911+0551 (Bade et al. 1997), MG 0751+2716 (Tonry & Kochanek 1999), SDSS J0903+5028 (Johnston et al. 2003), CLASS B1608+656 (Fassnacht et al. 2005), B2108+213 (McKean et al. 2005), and HE 0435−1223 (Morgan et al. 2005). If dense environments of the lens galaxies are common, then they could affect strong lens studies in several ways (Keeton & Zabludoff 2004). On the theoretical side, estimation of environmental effects remains controversial: While Keeton et al. (2000) and Holder & Schechter (2003) argued that the large fraction of lens systems should lie in dense environments and thus the environmental effects are significant, Dalal & Watson (2005) estimated, using a halo occupation distribution, that the typical values for the external convergence and shear are quite small. Although we have already seen in §§ 3 and 4 that SDSS J1001+5027 and SDSS J1206+4332 have additional galaxies that likely affect the lens potential, it is important to check the larger field for hints of groups or clusters.

Figure 6 shows the fields around the lens systems obtained at UH88. We find many galaxies around SDSS J1001+5027, indicating that there may be a group or cluster along the line of sight. For SDSS J1206+4332, we cannot see any noticeable enhancement of the number of galaxies around the lens system, although there are several faint galaxies near the lens system.

To explore the environments further, we derived the number densities of galaxies around each lens system using the UH88 images. We perform object identifications using the Source Extractor algorithm (SExtractor; Bertin & Arnouts 1996). We define galaxies as objects with SExtractor parameter CLASS_STAR smaller than 0.6 in the *I*-band image. Note that this star/galaxy separation criterion is successful only for objects with $I \lesssim 22$. We derive the number densities of galaxies as a function of *I*-band magnitudes of the galaxies, which are shown in Figure 7. In the figure, we compare the galaxy number densities within 60″ of each lens system with those of the background, estimated from galaxies more than 60″ away in each image after excluding the region near bright stars. The total areas of the backgrounds are thus 87.0 and 79.8 arcmin^2 for SDSS J1001+5027 and SDSS J1206+4332, respectively. We find an enhancement of galaxy number densities for SDSS J1001+5027; the number densities of three magnitude bins show excesses by more than 1 σ. On the other hand, the galaxy number count around SDSS J1226+4332 is consistent with that of the background.

Figure 8 shows a color-magnitude diagram of galaxies near SDSS J1001+5027 to study the origin of the enhancement of galaxy number densities. We find a weak ridge line at $R - I \sim 0.75$, suggesting the existence of a group or a cluster at $z \sim 0.2$, which is consistent with that of lens galaxies G1 and G2 estimated from their colors. We also plot the distribution of galaxies at $z \gtrsim 0.2$ by making color cuts: $V - R > 0.9$, $R - I > 0.7$, and $I < 22$. We find that the galaxies are clustered north and west of the lens system, rather than distributed homogeneously (see also Fig. 6). Thus, the lens galaxy may lie in a group

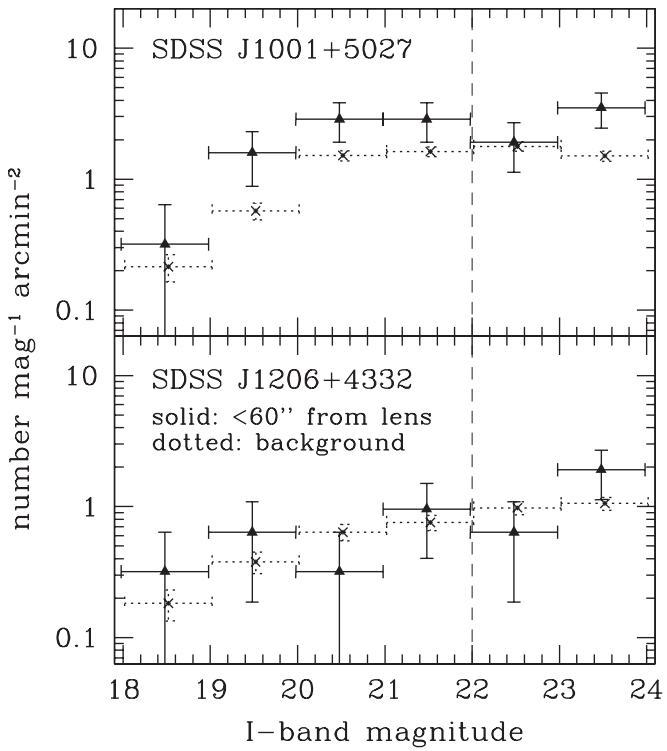

FIG. 7.—*I*-band galaxy number counts of fields within 60″ of the lens systems (*filled triangles with solid error bars*) as well as background counts (*crosses with dotted error bars*). The error bars include Poisson errors only. The vertical dashed lines indicate the approximate limit of the star/galaxy separation.

or a cluster that is located to the northwest of the lens; spectroscopic identifications of these galaxies as well as the lens galaxy should be undertaken.

6. IS THE NUMBER OF 3″ LENSES CONSISTENT WITH THEORY?

Thus far, 13 gravitationally lensed quasars have been discovered using the SDSS. In addition, we have recovered several previously known lensed quasar systems. Table 4 summarizes the current status of our lens search in the SDSS. Note that limitations of follow-up time have forced us to focus on the SDSS spectroscopic sample of quasars.[20] Thus, the list does not contain lenses that do not have SDSS spectra (e.g., APM 08279+5255; see Pindor et al. 2003). The table does not contain SDSS J1402+6321 (Bolton et al. 2005) either, since the redshift ($z = 0.48$) is below our criterion for the quasar sample (see discussion below). Among gravitational lenses in the table, SDSS J1004+4112 and Q0957+561 were selected by searching around each quasar for stellar objects that have similar colors as the quasar itself (Oguri et al. 2004a; Hennawi 2004), and the rest were successfully selected by our standard candidate selection algorithm (see § 2), although the first identifications of some of the candidates were made by different algorithms. An exception is SDSS J0903+5028 (Johnston et al. 2003), which was targeted as a luminous red galaxy (Eisenstein et al. 2001) because of the bright lens galaxy; however, we include this system in the statistical analysis below, since the quasar would have been targeted as a high-redshift quasar if it had not been obscured by the foreground lens galaxy (Richards et al. 2002). The table shows that we have discovered a relatively large number of $\sim$3″ lenses. We note that our current lens sample shown in Table 4 is quite incomplete,[21] and that future follow-up observations would increase the number of lenses even in the current quasar sample. Therefore we now calculate the expected lensing probability in the SDSS quasar sample and compare it with the number of $\sim$3″ lenses in the sample. In particular, we neglect the contribution of lens galaxy environments, as has normally been done, to see whether the assumption is still valid. In computing the lensing probability, we assume a spatially flat universe ($\Omega_M + \Omega_\Lambda = 1$).

We compute the lensing probability distribution along the lines described by Turner et al. (1984). The lens galaxies are

[20] The photometric quasar sample (Richards et al. 2004) has an order of magnitude more quasars than the spectroscopic sample and thus is expected to contain many more lenses.

[21] We note that our follow-up observations are biased against discovering lensed quasars with separations <2″ because of poor seeing in many follow-up observations. This mostly explains the large discrepancy between theory and observation at the image separation range.

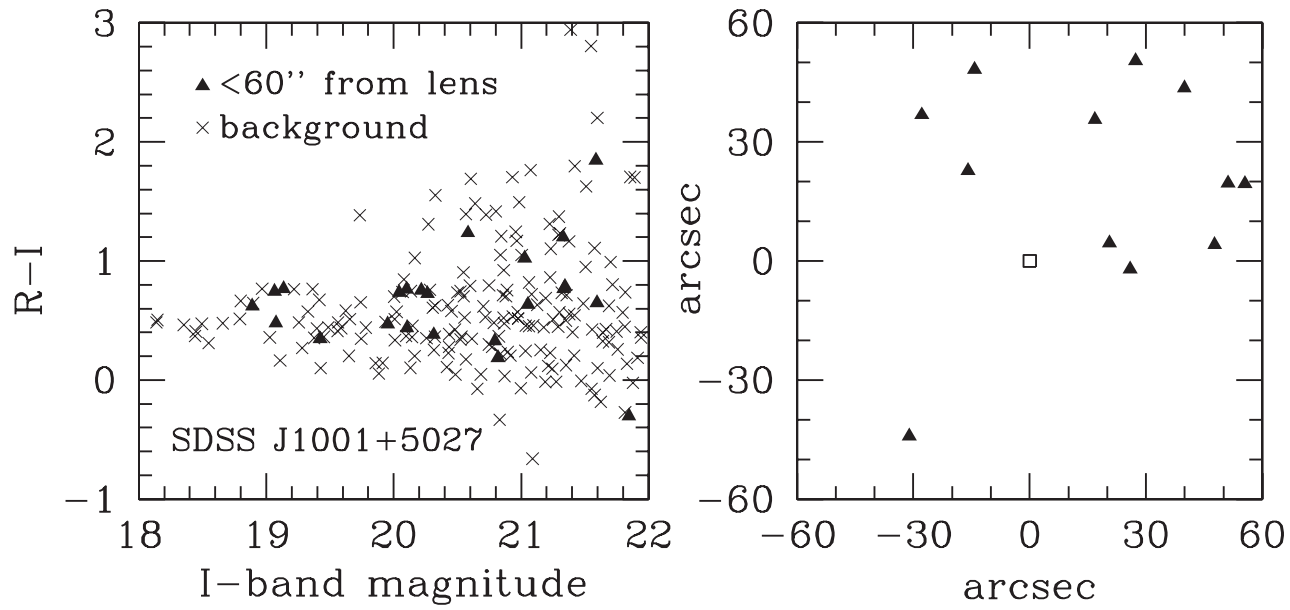

FIG. 8.—*Left*: Color-magnitude diagrams of galaxies in the field within 60″ of SDSS J1001+5027 (*filled triangles*) and the background (*crosses*). *Right*: The distribution of galaxies at $z \gtrsim 0.2$ (*filled triangles*) around the lens system SDSS J1001+5027 (*open square*). North is up, and east is to the left.

TABLE 4
GRAVITATIONALLY LENSED QUASARS (RE-)DISCOVERED IN THE SDSS: CURRENT STATUS

Name	θ_{max}[a] (arcsec)	z_s	z_l	Comments	Reference
Q0142−100	2.22	2.72	0.49	Previously known lens	1
SDSS J0246−0825	1.04	1.69	0.72?	...	2
SDSS J0903+5028	2.83	3.58	0.39	Targeted as a galaxy	3
RX J0911+0551	3.25	2.80	0.77	Previously known lens	4
SBS 0909+523	1.11	1.38	0.83	Previously known lens	5
SDSS J0924+0219	1.78	1.52	...	...	6
Q0957+561	6.17	1.41	0.36	Previously known lens	7
SDSS J1001+5027	2.86	1.84	...	...	8
SDSS J1004+4112	14.62	1.73	0.68	Large separation lens	9
SDSS J1021+4913	1.05	1.72	...	...	10
PG 1115+080	2.43	1.72	0.31	Previously known lens	11
SDSS J1138+0314	1.46	2.44	...	...	12
SDSS J1155+6346	1.83	2.89	0.18?	...	13
SDSS J1206+4332	2.90	1.79	0.75?	...	8
SDSS J1226−0006	1.24	1.13	0.52?	...	14
SDSS J1335+0118	1.56	1.57	...	...	15
SDSS J1650+4251	1.18	1.55	...	...	16

NOTES.—The SDSS strongly lensed quasar survey is still ongoing, and we have many other candidates requiring follow-up observations. Therefore, this list is far from complete. This list includes only lenses that have SDSS spectra.

[a] The maximum separation between multiple images in arcseconds.

REFERENCES.—(1) Surdej et al. 1987; (2) Inada et al. 2005b; (3) Johnston et al. 2003; (4) Bade et al. 1997; (5) Oscoz et al. 1997; (6) Inada et al. 2003a; (7) Walsh et al. 1979; (8) this paper; (9) Inada et al. 2003b; (10) B. Pindor et al. 2005, in preparation; (11) Weymann et al. 1980; (12) S. Burles et al. 2005, in preparation; (13) Pindor et al. 2004; (14) Inada et al. 2005a; (15) Oguri et al. 2004b; (16) Morgan et al. 2003.

modeled by SIS $\rho(r) = \sigma^2/(2\pi G r^2)$, where σ is the velocity dispersion of the lens galaxy. We adopt the velocity function of early-type galaxies determined from ∼30,000 SDSS galaxies at $0.01 < z < 0.3$ (Sheth et al. 2003; M. Bernardi et al. 2005, in preparation; Mitchell et al. 2005) and neglect the redshift evolution (i.e., we assume that the velocity function is constant in comoving units). The use of the velocity function of early-type galaxies is sufficient for our calculation because at $\theta \gtrsim 3''$ lensing by early-type galaxies is dominant (Turner et al. 1984). We also need to incorporate the selection function of the SDSS lens search, which we do in a preliminary way by making the following assumptions. First, we use the magnification factor of the brighter image, $\mu_{bright} = (\theta_E/\theta_S) + 1$, where θ_E is the Einstein radius and θ_S is the position of the source relative to the lens galaxy, to compute the magnification bias, because at $\theta \gtrsim 3''$ two lensed components are well separated in the SDSS data. Although we may have an alternative choice of using the magnification factor of the fainter image, we adopt μ_{bright} to calculate the upper limit of the lensing probability; thus the actual lensing rate at $\theta \gtrsim 3''$ might be smaller than our calculation.[22] Next, for the limiting bright-to-faint flux ratio we assume $f_{max} = 10$; this is justified because all of the lenses in Table 4 satisfy this condition. Lensing probabilities calculated with this selection function represent an upper limit at a relatively large image separation $\theta \sim 3''$.

To calculate the expected number of lensed quasars in the current SDSS quasar sample, we need the luminosity function of quasars as well as the redshift and magnitude distributions of the quasar sample. We adopt a sample of ∼47,000 quasars at $0.6 < z < 4.0$. The sample is constructed in the same way as in Oguri et al. (2004a). We did not search for lensed quasars at $z < 0.6$, as low-redshift quasars are intrinsically extended, and we do not use high-redshift quasar ($z > 4.0$) sample because it contains a significant fraction of objects whose spectra were misidentified by the SDSS spectroscopic pipeline (see discussion in Schneider et al. 2003). The redshift distribution is similar to that shown in Oguri et al. (2004a). For the luminosity function of quasars, we use what is called LF1 in Oguri et al. (2004a), which has a faint end slope of 1.64 and a bright end slope of 3.43 ($z < 3$) or 2.58 ($z > 3$).

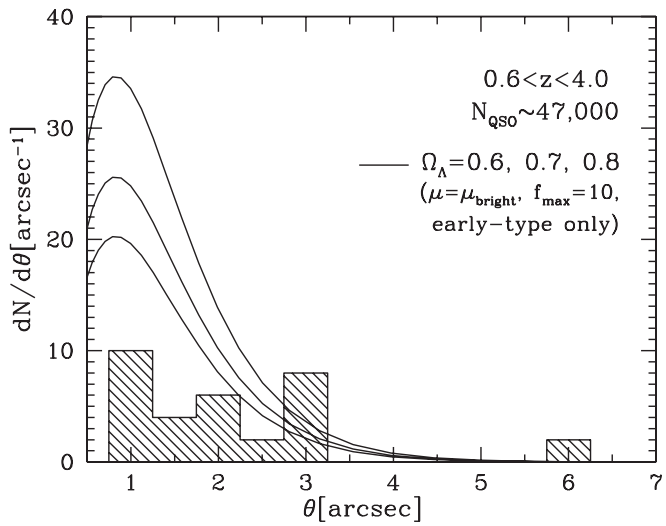

FIG. 9.—Tentative comparison of image separation distributions of lensed quasars in the current SDSS quasar sample. Lines show the theoretical expectations (see text for details of computation) using an SIS model, for different values of the cosmological constant, $\Omega_\Lambda = 0.6$, 0.7, and 0.8 from bottom to top, respectively. Shaded region indicates the distribution of all lensed quasars discovered and recovered in the SDSS (see Table 4). The large separation lensed quasar SDSS J1004+4112 ($\theta = 146$) is not included in this plot.

[22] Note that at smaller separation ($\theta \sim 1''$) our computation is expected to underestimate the lensing probability because at such small separations lensed components are not decomposed, and thus the magnification factor of the two images $\mu_{total} = 2\theta_E/\theta_S$ is more appropriate.

The result is shown in Figure 9. As can be seen, the number of $\sim 3''$ lenses already exceeds the theoretical expectations, when we adopt the standard value of the cosmological constant, $\Omega_\Lambda \sim 0.7$. The situation is similar if we increase Ω_Λ to 0.8. In terms of the constraint on the cosmological constant, the excess in the bin centered at $\theta = 3''$ is described as $\Omega_\Lambda > 0.90$ (68% confidence limit) assuming a Poisson distribution, which is highly inconsistent with recent measurements of the cosmological constant $\Omega_\Lambda \sim 0.70$ with errors of less than 10% (e.g., Tegmark et al. 2004). We emphasize that our current lens sample is quite incomplete; indeed, currently we have several $\sim 3''$ quasar pairs with the same redshifts that could also be gravitational lenses (Hennawi 2004), which need deep imaging to find the putative lens galaxies. Thus, observations of these quasar pairs as well as lens candidates should be conducted, which might make the discrepancy even larger. Such an excess may indicate that our simple treatment of lensing statistics is inaccurate and that we need to include other effects.

7. SUMMARY

We report the discovery of two gravitationally lensed quasars, SDSS J1001+5027 and SDSS J1206+4332. The systems were identified as new lens candidates in the SDSS and confirmed as lenses by spectroscopic and imaging observations at the ARC 3.5 m and UH88 telescopes. SDSS J1001+5027 is a lensed quasar at $z = 1.838$ and consists of two lensed images separated by $2''.86$. SDSS J1206+4332 is a lensed quasar at $z = 1.789$ and consists of two lensed images separated by $2''.90$. In each system we have identified the galaxy responsible for the lensing.

We have found that the lens systems are complicated. The imaging data clearly show other galaxies that are very close to the main lens galaxies. The lens modeling has shown that these galaxies affect the lens potentials significantly. We have examined the wide-field images, which show an enhancement of the galaxy number density within $60''$ of SDSS J1001+5027. Spectroscopic follow-up observations are needed to see if the group/cluster ($z \sim 0.2$) is actually associated with the lens galaxy.

Although the SDSS lens survey is ongoing, we have made a preliminary comparison of theoretical lensing probability distributions with the observed distribution. We have found that the number of lenses with $\theta \sim 3''$ already exceeds the theoretical expectations. We still have many lens candidates with $\theta \gtrsim 3''$ that remain to be observed (Hennawi 2004); if some of them turn out to be true gravitational lenses, the conflict will become even stronger. This excess may be caused by external convergence and shear fields, which we have not taken into account in our calculation. Basically, external shear broadens the distribution of image separations for a given mass of a lens object (e.g., Huterer et al. 2005). This broadening is enough to enhance the lensing probability at $\theta \gtrsim 3''$ because the lensing probability at the image separation region is a strong function of image separations. More significant enhancement may be achieved by external convergence, since it increases both image separation and lensing probability. Indeed, among five intermediate separation lenses in Table 4, two lens systems (RX J0911+0551 and Q0957+561) lie in clusters, and two other lens systems (SDSS J0903+5028 and SDSS J1001+5027) also appear to lie in dense environments. In addition, the two lens systems reported in this paper are complex, in the sense that galaxies very close to the main lens galaxies affect the lens potentials. Other possible systematic effects include triaxiality of lenses (Oguri & Keeton 2004) and massive substructures (Cohn & Kochanek 2004). In either case, lens statistics at this image separation should be done with caution; simple models that consider only isolated single lens objects can be misleading.

We thank Paul Schechter for useful comments and the anonymous referee for many suggestions. M. O. and N. I. are supported by the JSPS through the JSPS Research Fellowship for Young Scientists. J. F. H. is currently supported by NASA through Hubble Fellowship grant 01172.01-A, awarded by the Space Telescope Science Institute, which is operated by the Association of Universities for Research in Astronomy, Inc., for NASA, under contract NAS 5-26555. Funding for the creation and distribution of the SDSS Archive has been provided by the Alfred P. Sloan Foundation, the Participating Institutions, the National Aeronautics and Space Administration, the National Science Foundation, the US Department of Energy, the Japanese Monbukagakusho, and the Max Planck Society. The SDSS Web site is http://www.sdss.org. The SDSS is managed by the Astrophysical Research Consortium (ARC) for the Participating Institutions. The Participating Institutions are the University of Chicago, Fermilab, the Institute for Advanced Study, the Japan Participation Group, The Johns Hopkins University, the Korean Scientist Group, the Los Alamos National Laboratory, the Max-Planck-Institute for Astronomy (MPIA), the Max-Planck-Institute for Astrophysics (MPA), New Mexico State University, the University of Pittsburgh, Princeton University, the United States Naval Observatory, and the University of Washington. This work is based on observations obtained with the Apache Point Observatory 3.5 m telescope, which is owned and operated by the Astrophysical Research Consortium, and with the University of Hawaii 2.2 m telescope.

REFERENCES

Abazajian, K., et al. 2003, AJ, 126, 2081
———. 2004, AJ, 128, 502
———. 2005, AJ, 129, 1755
Bade, N., Siebert, J., Lopez, S., Voges, W., & Reimers, D. 1997, A&A, 317, L13
Bertin, E., & Arnouts, S. 1996, A&AS, 117, 393
Blanton, M. R., Lin, H., Lupton, R. H., Maley, F. M., Young, N., Zehavi, I., & Loveday, J. 2003, AJ, 125, 2276
Bolton, A. S., Burles, S., Koopmans, L. V. E., Treu, T., & Moustakas, L. A. 2005, ApJ, submitted (astro-ph/0410425)
Browne, I. W. A., et al. 2003, MNRAS, 341, 13
Cohn, J. D., & Kochanek, C. S. 2004, ApJ, 608, 25
Dalal, N., & Watson, C. R. 2005, ApJ, submitted (astro-ph/0409483)
Eisenstein, D. J., et al. 2001, AJ, 122, 2267
Fassnacht, C., et al. 2005, in Proc. IAU Symp. 225, Impact of Gravitational Lensing on Cosmology, ed. Y. Mellier & G. Meylan (Cambridge: Cambridge Univ. Press), in press (astro-ph/0409086)
Faure, C., Alloin, D., Kneib, J.-P., & Courbin, F. 2004, A&A, 428, 741
Fukugita, M., Ichikawa, T., Gunn, J. E., Doi, M., Shimasaku, K., & Schneider, D. P. 1996, AJ, 111, 1748
Fukugita, M., Shimasaku, K., & Ichikawa, T. 1995, PASP, 107, 945
Gunn, J. E., et al. 1998, AJ, 116, 3040
Hennawi, J. F., 2004, Ph.D. thesis, Princeton Univ.
Hogg, D. W., Finkbeiner, D. P., Schlegel, D. J., & Gunn, J. E. 2001, AJ, 122, 2129
Holder, G. P., & Schechter, P. L. 2003, ApJ, 589, 688
Huterer, D., Keeton, C., & Ma, C. 2005, ApJ, submitted (astro-ph/0405040)
Inada, N., et al. 2003a, AJ, 126, 666
———. 2003b, Nature, 426, 810
———. 2005a, AJ, submitted
———. 2005b, AJ, submitted
Ivezić, Ž., et al. 2004, Astron. Nachr., 325, 583
Johnston, D. E., et al. 2003, AJ, 126, 2281

Keeton, C. R. 2001, ApJ, submitted (astro-ph/0102340)
Keeton, C. R., Christlein, D., & Zabludoff, A. I. 2000, ApJ, 545, 129
Keeton, C. R., Kochanek, C. S., & Falco, E. E. 1998, ApJ, 509, 561
Keeton, C. R., & Zabludoff, A. I. 2004, ApJ, 612, 660
Landolt, A. U. 1992, AJ, 104, 340
Lawrence, C. R., Schneider, D. P., Schmidt, M., Bennett, C. L., Hewitt, J. N., Burke, B. F., Turner, E. L., & Gunn, J. E. 1984, Science, 223, 46
Lupton, R., Gunn, J. E., Ivezić, Z., Knapp, G. R., Kent, S., & Yasuda, N. 2001, in ASP Conf. Ser. 238, Astronomical Data Analysis Software and Systems X, ed. F. R. Harnden, Jr., F. A. Primini, & H. E. Payne (San Francisco: ASP), 269
Martel, H., Premadi, P., & Matzner, R. 2002, ApJ, 570, 17
McKean, J. P., et al. 2005, MNRAS, 356, 1009
Mitchell, J. L., Keeton, C. R., Frieman, J. A., & Sheth, R. K. 2005, ApJ, 622, 81
Morgan, N. D., Kochanek, C. S., Pevunova, O., & Schechter, P. L. 2005, AJ, submitted (astro-ph/0410614)
Morgan, N. D., Snyder, J. A., & Reens, L. H. 2003, AJ, 126, 2145
Myers, S. T., et al. 2003, MNRAS, 341, 1
Oguri, M. 2002, ApJ, 580, 2
Oguri, M., & Keeton, C. R. 2004, ApJ, 610, 663
Oguri, M., et al. 2004a, ApJ, 605, 78
———. 2004b, PASJ, 56, 399
Oscoz, A., Serra-Ricart, M., Mediavilla, E., Buitrago, J., & Goicoechea, L. J. 1997, ApJ, 491, L7
Pier, J. R., Munn, J. A., Hindsley, R. B., Hennessy, G. S., Kent, S. M., Lupton, R. H., & Ivezić, Ž. 2003, AJ, 125, 1559
Pindor, B., Turner, E. L., Lupton, R. H., & Brinkmann, J. 2003, AJ, 125, 2325
Pindor, B., et al. 2004, AJ, 127, 1318
Richards, G. T., et al. 2002, AJ, 123, 2945
———. 2004, ApJS, 155, 257
Schneider, D. P., et al. 2003, AJ, 126, 2579
Sheth, R. K., et al. 2003, ApJ, 594, 225
Smith, J. A., et al. 2002, AJ, 123, 2121
Stoughton, C., et al. 2002, AJ, 123, 485
Strauss, M. A., et al. 2002, AJ, 124, 1810
Surdej, J., Swings, J.-P., Magain, P., Courvoisier, T. J.-L., & Borgeest, U. 1987, Nature, 329, 695
Tegmark, M., et al. 2004, Phys. Rev. D, 69, 103501
Tonry, J. L., & Kochanek, C. S. 1999, AJ, 117, 2034
Turner, E. L., Ostriker, J. P., & Gott, J. R. 1984, ApJ, 284, 1
Walsh, D., Carswell, R. F., & Weymann, R. J. 1979, Nature, 279, 381
Wambsganss, J., Bode, P., & Ostriker, J. P. 2005, ApJ, submitted (astro-ph/0405147)
Weymann, R. J., et al. 1980, Nature, 285, 641
York, D. G., et al. 2000, AJ, 120, 1579